Journal of The Electrochemical Society, **154** (5) H384-H388 (2007)
0013-4651/2007/154(5)/H384/5/$20.00 © The Electrochemical Society

Plasma-Induced Damage Influence on the n-Contact Properties and Device Performance of Ultraviolet InGaN/AlGaN Light-Emitting Diodes

Sang-Mook Kim,[a,c] Young-Moon Yu,[a] Jong-Hyub Baek,[a] Seong-Ran Jeon,[b] Hyo-Jin Ahn,[c] and Ja-Soon Jang[d,*,z]

[a]*Korea Photonics Technology Institute, Gwangju 500-460, Korea*
[b]*LED Research and Development Lab, LG Electronics Institute of Technology, Seoul 137-724, Korea*
[c]*Department of Materials Science and Engineering, Gwangju Institute of Science and Technology, Gwanju 500-712, Korea*
[d]*Department of Electrical and Computer Engineering, Rutgers, The State University of New Jersey, Piscataway, New Jersey 08854, USA*

We report on plasma-induced-damage influence on the n-ohmic contact properties and device performance of ultraviolet InGaN/AlGaN light-emitting diodes (LEDs). A significant plasma-power dependence of n-ohmic contacts on electrical properties could be due to the generation of different types of point defects and movement of the surface Fermi level, which were confirmed by photoluminescence and X-ray photoelectron spectroscopy measurement. Unlike the low plasma-power-etched LED, the high plasma-power-etching in the LED results in an increase of the high threshold voltage, series resistance, and reverse leakage current. In addition, the current crowding in the plasma-damaged LEDs occurs even at low injection current of 5 mA, while that for the low plasma-power-etched LED does not happen. These different device characteristics are described and discussed in terms of the resistivity of the GaN and ohmic contacts and the current spreading length (from p- to n-GaN layer).
 [DOI: 10.1149/1.2712139]

Manuscript submitted November 20, 2006; revised manuscript received January 9, 2007. Available electronically March 19, 2007.

High-performance GaN-based light-emitting diodes (LEDs) with high efficiency and high reliability are of technological importance for applications in traffic signal, full color display, and solid state lighting.[1] To achieve a highly efficient and reliable LED, the enhancement of output power, and the reduction of the series resistance and the leakage current of LEDs are essential. However, it is known that GaN-based LEDs with a lateral current path suffer from current crowding and high series resistance due to the high contact resistance of p-type ohmic contacts.[2] In addition, the electrical properties of this spreading electrode are severely affected by the high resistivity of p-GaN, resulting in the high turn-on voltage of the LED.[3] High series resistance can give rise to the occurrence of current crowding and an increase of junction temperature, and hence degrade the electrical and optical properties of LED performance during device operation.[3,4] Furthermore, a high leakage current which may result from various defects such as vacancy and dislocation can also yield to the degradation of the device reliability.[5] Thus, it is crucial to reduce the contact resistance of p-ohmic electrode, the resistivity of p-GaN, and the number of defects. However, these issues could be valid assuming that the n-specific contact resistance and the n-GaN cladding layer resistivity are low enough to be negligible. Although several studies on effects of p-contact resistance and the resistivity of p-GaN layer on the LED performance have been reported,[3,6] effects of the n-specific contact resistance and the n-GaN cladding layer resistivity on the performance of GaN-based UV LEDs have not been clearly understood as yet.

As for plasma-induced damage on GaN-based materials, various works have been reported to investigate optimal etching conditions and their mechanisms for the formation of plasma-damaged surface of the (Al)GaN.[7-11] From these results, the origin of the plasma-induced damage is due to the formation of an element-deficient surface of the (Al)GaN layer. Although many reported studies for the plasma-induced damage influence on electrical and structural characteristics of the (Al)GaN have been successfully demonstrated and carried out, little research has been conducted to describe better understanding of both an annealing dependence on the electrical characteristics of the n-ohmic contacts (on the different plasma-power-etched GaN) and the plasma-induced damage effect on the LED performance characteristics such as current spreading length and current crowding.

In this paper, we report on the effect of the n-contact resistance and n-GaN cladding layer resistivity on the device-performance characteristics of UV LEDs. To study this work, during the mesa etching process, we fabricated low- and high-resistive GaN cladding layers of the LEDs using different plasma power conditions (in Table I). It is shown that the electrical and thermal properties of the ohmic contacts are considerably dependent on the different surface structure of the etched GaN. It is further shown that the series resistance, leakage current, optical power, and current crowding are considerably affected by an increase of n-specific contact resistance and the resistivity of n-cladding layer resulting from the plasma-induced damage.

Experimental

A metallorganic chemical vapor deposition (MOCVD) system was used to grow InGaN/AlGaN multiple quantum well (MQW) LED structures (having a peak wavelength of around 362 nm) on c-face sapphire substrates, as shown in Fig. 1. The LED structure consists of a 30 nm thick GaN nucleation layer grown on the sapphire substrate, a 2 μm thick unintentionally doped GaN layer, a 1.5 μm thick Si-doped GaN n-cladding layer ($N_d \sim 3 \times 10^{18}$ cm^{-3}), an active region with five periods of InGaN/AlGaN MQWs, a 0.15 μm thick Mg-doped GaN layer (p-GaN, $N_a \sim 3 \times 10^{17}$ cm^{-3}), and a 10 nm thick Mg-doped GaN layer (p$^+$-GaN, $N_a \sim 2 \times 10^{18}$ cm^{-3}). Prior to the fabrication of LEDs, the surface

Table I. Summary of the plasma etching conditions for the formation of mesa structure of the LEDs.

Sample	Description	Plasma etching condition
A	Low plasma-power etching	ICP/rf = 1000/30 W Etch rate = 0.12 mm/min Operation time = 5 min for etch depth of 0.6 mm
B	High plasma-power etching	ICP/rf = 2000/100 W Etch rate of 0.36 mm/min Operation time of 1 min 40 s for etch depth of 0.6 mm

* Electrochemical Society Active Member.
z E-mail: jjscontact@yahoo.co.kr

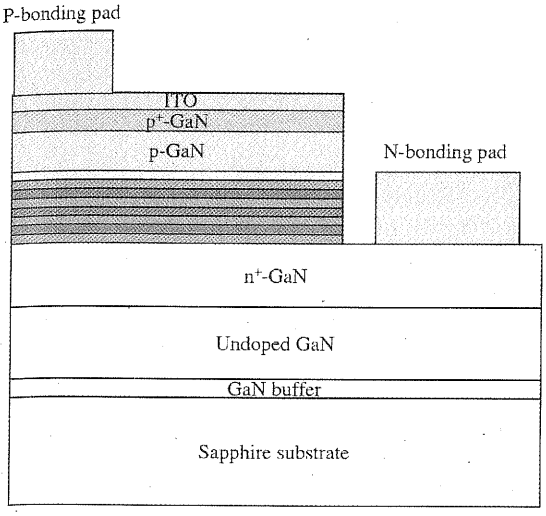

Figure 1. (Color online) Cross-sectional schematic of a InGaN/AlGaN MQWs LED.

of the LED samples was ultrasonically degreased with acetone, ethanol, and ethanol for 5 min in each step, and then rinsed with deionized water (DI). All LEDs (330 μm × 330 μm) were fabricated using photolithography patterning and inductive coupled plasma (ICP) etching with an etching depth of 0.6 μm. In this mesa etching process, we fabricated a low-resistive and a high-resistive n-GaN cladding layers of the LEDs using a low and a high ICP and radio-frequency (rf) power, respectively. The detailed etching conditions are summarized in Table I. For simplicity, a LED with the low-resistive n-cladding layer is referred here as a A-contact LED, while a LED having the high-resistive n-cladding layer referred as a B-contact LED. Sputtered ITO (220 nm) layers were used as p-type transparent ohmic electrodes for the A- and B-contact LEDs. All samples were rapid-thermal-annealed at 550°C for 1 min in a flowing N_2 ambient to form p-type ohmic contacts. For both LEDs, Cr/Ni/Au (20/30/500 nm) (as a n-ohmic electrode) was deposited on the *n*-GaN surface and Ni/Au (30/500 nm) (as a p-ohmic bonding pad) was deposited on the surface of the transparent ITO ohmic electrode. All samples were subsequently rapid-thermal-annealed at 500°C for 30 s in a flowing N_2 ambient. Current-voltage (*I-V*) data were measured using a semiconductor parameter analyzer (HP4155A). Electroluminescence and optical power were obtained using an optical spectrometer and a photodiode detector.

Results and Discussion

Plasma power effects on the electrical properties of n-GaN layers and n-ohmic contacts.— Hall-effect measurement was carried out to investigate the effect of plasma power on the sheet carrier concentration of the samples. The measurement showed that the sheet resistance of the as-grown, low plasma-power-etched (A sample, in Table I), and high plasma-power-etched GaN (B sample) is 31.2(±1.2), 19.7(±1.1), and 87.3(±1.3) Ω/□, respectively. This indicates that electrical properties of the samples are sensitively affected by ICP and rf plasma power conditions. Note that the sheet resistance of the A sample is somewhat reduced as compared to that of the as-grown sample, while that of the B sample is considerably increased.

Figure 2a shows the photoluminescence (PL) characteristics of the low and the high plasma-power-etched GaN (A and B sample). It is shown that a band-to-band transition peak without any yellow band peak is observed on the A sample. For the B sample, however, a broad yellow-energy-band peak of 2.1 (±0.15) eV as well as a band-to-band peak is detected, indicating that the formation of deep-level defects.[8,9,12,13]

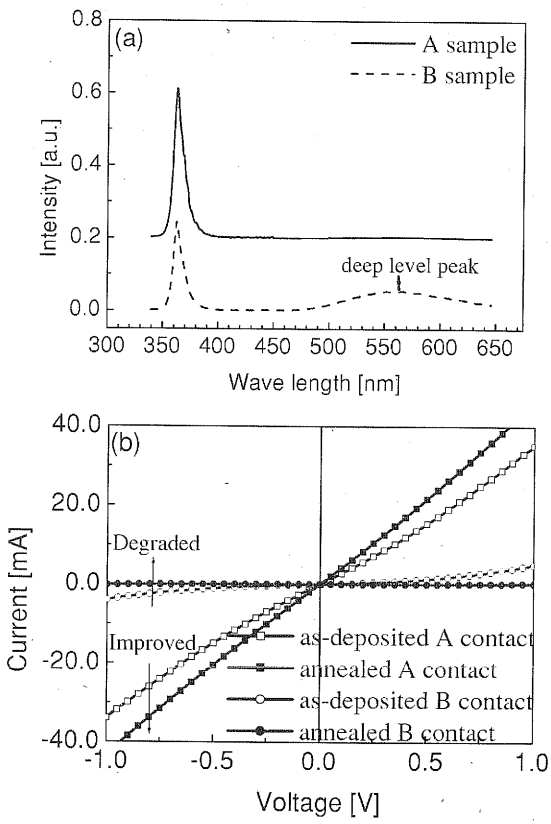

Figure 2. (a) Photoluminescence characteristics of high and low plasma-power-etched GaN. (b) Current-voltage characteristics of Cr/Ni/Au ohmic contacts to the high and low plasma-power-etched GaN before and after annealing.

Figure 2b shows the *I-V* characteristics of the Cr/Ni/Au ohmic contacts on the A and the B sample layer before and after annealing. For this work, circular-transmission line model (CTLM) patterns were fabricated using a photolithography and lift-off process. It is shown that the *I-V* characteristics of the A contact become improved after annealing at 500°C for 30 s, whereas that of the B contact is thermally degraded after annealing. Specific contact resistance (R_{sc}) was determined from a plot of the measured resistances versus spacings between CTLM pads. CTLM method was used to fit a log-scaled line to the experimental data.[14] Calculations showed that for the A contact, R_{sc} is determined to be 8.1 (±0.1) × 10^{-5} and 6.4 (±0.2) × 10^{-6} Ω cm^2 before and after annealing, respectively, while for the B contact R_{sc} is 8.8 (±0.2) × 10^{-2} and 2.3 (±0.2) Ω cm^2 before and after annealing, respectively. The different behavior of the annealing-temperature dependence on the electrical properties of the A and the B contact may be associated with the different surface condition of the etched GaN layer by the different etching-power condition (Table I) and are described later.

To investigate the plasma power effect on the surface atomic composition and the surface Fermi level of both the samples, X-ray photoelectron spectroscopy (XPS, MultiLab 2000 model) was carried out using an Al Kα X-ray source in the ultrahigh vacuum chamber. In this work, all core-level peaks were calibrated using a reference peak of Au 4f. When the Ga/N ratio of the as-grown n-GaN set as 1, it was shown that the Ga/N ratio of the A sample was determined to be 1.33(±0.03) while that of the B sample was calculated to be 0.87(±0.03). This describes that the low and high plasma-power etching produces nitrogen (V_N) and gallium vacancies (V_{Ga}) near the surface of the A sample and B sample, respectively. In addition, it is shown that the Ga 3d core-level peak of the A sample shifts toward high binding-energy side by an energy of 0.23 eV as

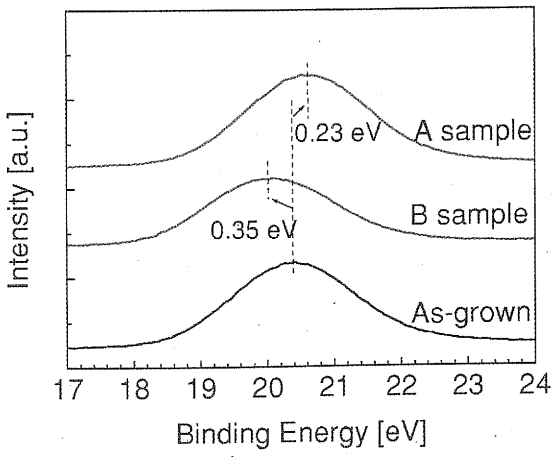

Figure 3. (Color online) Photoelectron spectra of the Ga 3d core-level for the as-grown, high and low plasma-power-etched GaN.

compared to that of the as-grown sample (Fig. 3), indicating that the surface Fermi level moves toward the conduction band minimum (CBM) edge.[15,16] On the contrary, the Ga 3d core-level peak of the B sample moves toward the low binding-energy side by an energy of 0.35 eV, indicating that the surface Fermi level towards the valence band maximum (VBM) edge.[15,16] It is well known that a nitrogen vacancy acts as a donor and a gallium vacancy as a deep acceptor.[12,13,17] Therefore, the shift of the surface Fermi level toward high binding-energy side in the A sample could be due to an increase of carrier concentration (originating from the generation of V_N near the surface). However, as for the B sample, a high density of V_{Ga} in the GaN surface can lead to an increase of the self-compensation between the donors and deep-level-acceptors, resulting in the shift of the surface Fermi level toward VBM edge.

Based on the Hall-effect, PL, *I-V* data of the contacts, and XPS results, a low sheet resistance of the A sample could be due to an increase of carrier concentration near the surface, whereas a high sheet resistance of the B sample could be attributed to an increase of the self-compensation. Furthermore, the different contact properties of both the as-deposited contacts could be due to the different movement of the surface Fermi level toward CBM or VBM edge.

The different behaviors for the annealing dependence on the *I-V* characteristics in both the contacts may be related to different interfacial reactions. Glancing angle X-ray diffraction results (GXRD), not shown here, showed that Cr_2N phase is formed at the Cr/GaN (A sample) interface upon annealing at 500°C. However, it was found that annealing produces CrGa phase as well as Cr_2N at the interface between the Cr and GaN (B). From the GXRD results, an improvement in the annealed A contact may be attributed to an increase of donor concentration by a further increase of nitrogen vacancies near the GaN region. In the case of the annealed B contact, however, the thermal degradation may be attributed to the further enhancement of the self-compensation near the GaN surface, resulting from the interfacial reactions among the Cr, Ga, and N. Another possible mechanism for the thermal degradation may be due to the formation of large Schottky barrier height (SBH) by a Cr-Ga intermetallic phase. In general, for n-ohmic contacts, metal-nitride phases contribute to a reduction of the SBH, while metal-Ga phases lead to an increase of the SBH.[18-20]

Comparison of electrical/optical characteristics of the A- and B-contact LEDs.— Figure 4a shows the forward *I-V* characteristics of the A- and the B-contact LEDs. Turn-on voltage of the A-contact LED (at 20 mA) is measured to be 3.58 (±0.03) V, whereas that of the B-contact LED is 3.93 (±0.03) V. Note that the high plasma-power etching gives rise to a large deviation in the turn-on voltage by about 0.35 V. The slope of the *I-V* curves means series resistance

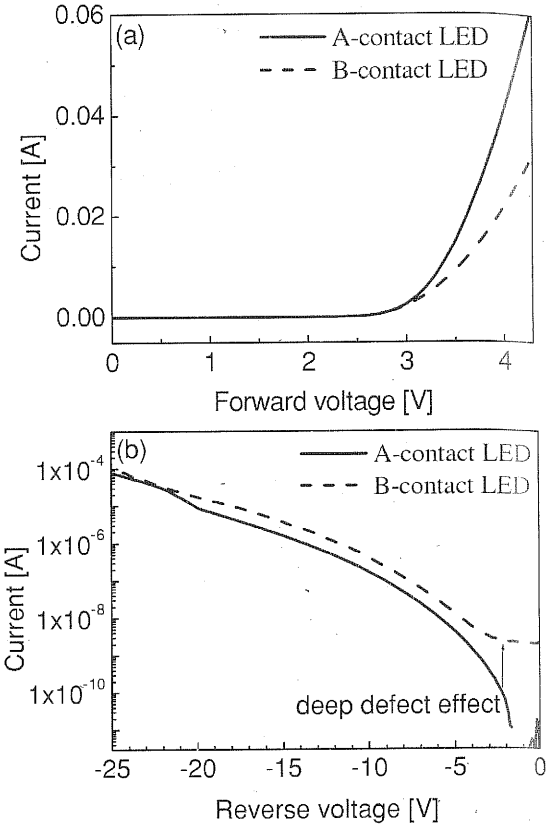

Figure 4. (a) Forward *I-V* characteristics of the A- and the B-contact LEDs. (b) Reverse *I-V* behaviors of both the LEDs.

which is one of the factors that can determine the quality of the LED performance. The series resistance of LEDs can be obtained using an equation given as[6]

$$I\left(\frac{dV}{dI}\right) = I \cdot R_s + \frac{nkT}{q} \qquad [1]$$

where n is the ideality factor, k Boltzmann constant, and R_s is the series resistance. Calculations show that the series resistance of an A-contact LED is 9.2 (±0.12) Ω, while that of B-contact LED is 21.3(±0.16) Ω. Notably, the series resistance of the A-contact LED is much lower than that of the B-contact LED, indicating that the resistance of n-GaN and n-ohmic contact plays an important role in affecting the series resistance. The ideality factor of the A-contact LED was determined to be 2.52 (±0.02), whereas that of the B-contact LED was 3.13 (±0.02). According to Cao et al.,[21] it was known that the ideality factor (with >2) could be due to the deep-level defects in the GaN-based LEDs. Even though the ideality factors of both the LEDs have more than 2, higher value of ideality factor in the B-contact LED may be associated with the generation of deep-level V_{Ga} defects, as described from PL and XPS results. It is further shown that the reverse leakage current of the B-contact LED is significantly increased at the reverse voltage regions of ≤−2.5 V as compared to that of the A-contact LED. Interestingly, the voltage region where the high reverse leakage current occurred is so similar to the energy region for the formation of deep level defects (Fig. 2a). Our findings imply that the deep-level defects in the B layer may act as a leakage path and hence contribute to an increase of the reverse leakage current.

Figure 5 shows the optical output power-current (*L-I*) characteristics of the A- and B-contact LEDs as a function of the injection current. A comparison of the *L-I* data shows that the output power of the A-contact LEDs (at 20 mA) is higher than that of the B-contact

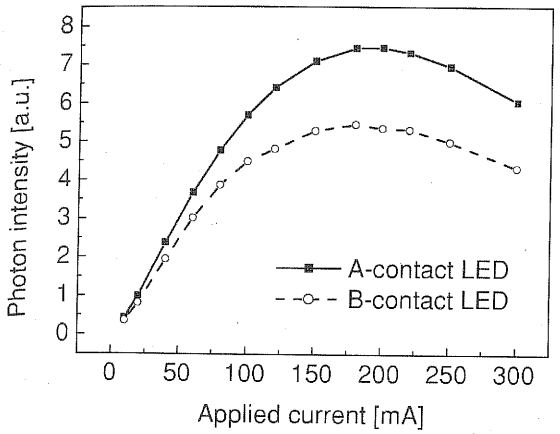

Figure 5. Optical output power-current (L-I) characteristics of the A- and B-contact LEDs as a function of the injection current.

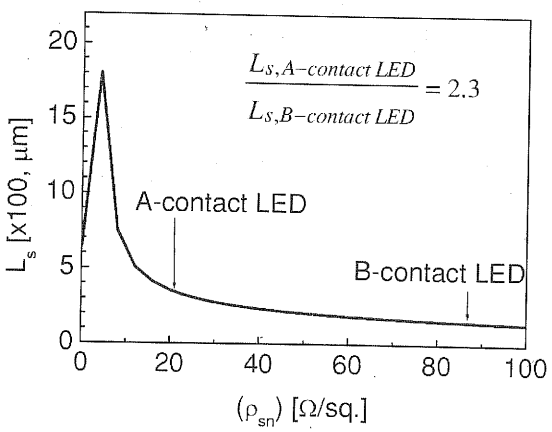

Figure 7. Plot of the spreading resistance vs sheet resistance of n-GaN. The calculation was carried out using the Eq. 2 and 3.

LED by ~20%. Unlike the A-contact LED, the B-contact LED shows the current crowding along the perimeter of n-ohmic electrode even at the low injection current of 5 mA as shown in Fig. 6. In this work, for both the samples we confirmed p-ohmic contact resistance of 4.0 (±0.4) × 10^{-3} Ω cm^2 and p-GaN resistivity 2.6(±0.3) Ω cm, which belong to normal characteristics. Therefore, the occurrence of current crowding in the B-contact LED may be due to the high resistance of plasma-damaged n-GaN and n-ohmic contact. Another possible mechanism for the current crowding may be attributed to the sidewall damage of the LED. During the mesa etching, a high ICP and rf power may give rise to sidewall damage as well as n-GaN surface damage.[22] A sidewall damage along the facet of the mesa may cause a generation of various types of defects that act as a carrier-trap center,[22,23] and hence result in the current crowding.

According to the theory of the GaN-based LED having a lateral current spreading path,[3,24-26] the current crowding and the total series resistance (R_{st}) can be subject to the sheet resistance of p-transparent ohmic electrode (ρ_{tp}), the p-specific contact resistance (ρ_{cp}), the resistivity of p-GaN cladding layer (ρ_p), n-specific contact resistance (ρ_{cn}) per unit length, the sheet resistance of n-GaN cladding layer (ρ_{sn}). In this case, the total series resistance (R_{st}) and the spreading length (L_s) are given by[25,26]

$$R_{st} = \rho_{tp}/3 + \rho_{cp}/L^2 + \rho_p t_p/L^2 + \rho_{sn}(L_s + d_{mn})/3L + \rho_{cn}/3L \quad [2]$$

$$L_s = \sqrt{\frac{(\rho_p + \rho_{cp})}{|\rho_{tp} - \rho_{sn}|}} \quad [3]$$

where d_{mn} is the spacing between the mesa and the n-ohmic electrode and L for the square mesa of sides. In this calculation, ρ_{tp} of 4.5 Ω/□, ρ_{cp} of 0.004 Ω cm^2, and ρ_p of 2.6 Ω cm, which were determined by Hall measurement and CTLM method, were employed. From the calculation, the value of L_s(A-contact LED)/L_s(B-contact LED) was determined to be 2.3 as shown in Fig. 7. In addition, the value of R_{st}(A-contact LED)/R_{st}(B-contact LED) was calculated to be 0.41 using Eq. 2 and 3, which is in good agreement with that calculated from the I-V data, indicating that our calculation is valid. From calculations, it is clearly shown that the high resistivity of n-GaN and high contact resistance of n-ohmic contact, originating from the plasma-induced damage, strongly affect an increase of series resistance and the reduction of current spreading length, and hence lead to the current crowding.

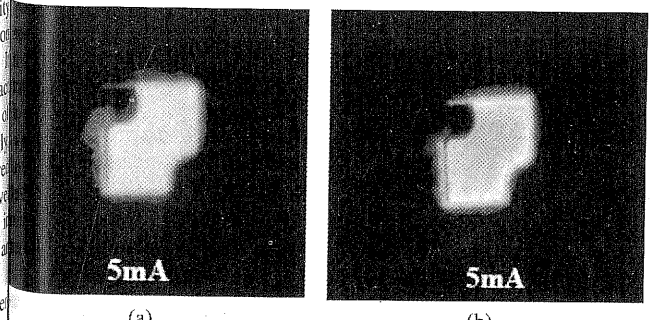

Figure 6. (Color online) Optical emission images obtained from (a) the A- and (b) B-contact LEDs.

Conclusions

We have investigated the plasma-induced damage influence of the n-ohmic contact and InGaN/AlGaN UV LED on the electrical and optical characteristics. Point defects caused by the high plasma-power give rise to the increase of the sheet resistance of n-GaN cladding layer and n-ohmic contact resistance. Especially, the annealing temperature dependence on the I-V characteristics of n-ohmic contacts on the different plasma-etched GaN clearly reveals that the metallurgical reaction between the metal and GaN is considerably dependent on the etched surface condition of the GaN. From the comparison of the low and high plasma-power-etched LEDs, it is shown that the LED etched by a high energy ion bombardment leads to high series resistance, high reverse leakage current under −3 V, and low optical power. These results produce the reduction of current spreading length and hence the occurrence of current crowding even at low current of 5 mA.

Acknowledgment

This work was financially supported by a Regional Innovation Project from the MOCIE, Korea.

KOPTI assisted in meeting the publication costs of this article.

References

1. S. Nakamura, S. Senoh, and N. Iwasa, *Jpn. J. Appl. Phys., Part 1*, **34**, L797 (1995).
2. Y. Nakano and T. Jimbo, *J. Appl. Phys.*, **92**, 5590 (2002).
3. X. Guo and E. F. Schubert, *Appl. Phys. Lett.*, 78, 3337 (2001).
4. J. Park and C. Lee, *IEEE Electron Device Lett.*, **26**, 308 (2005).
5. C. Y. Hsu, W. H. Lau, and Y. S. Wu, *Appl. Phys. Lett.*, **83**, 2447 (2003).
6. J.-S. Jang, D.-H. Kim, and T.-Y. Seong, *IEEE Photon. Technol. Lett.*, **18**, 1536 (2006).
7. X. A. Cao, S. J. Pearton, A. P. Zhang, G. T. Dong, F. Ren, R. Hickman, and J. M. Van Hove, *Appl. Phys. Lett.*, **75**, 2569 (1999).
8. H. W. Choi and S. J. Chua, *Phys. Status Solidi A*, **188**, 393 (2001).
9. K. J. Choi, H. W. Jang, and J.-L. Lee, *Appl. Phys. Lett.*, **82**, 1233 (2003).
10. Q. Fan, S. Chevtchenko, X. Ni, S.-J. Cho, F. Yun, and H. Morkoc, *J. Vac. Sci. Technol. B*, **24**, 1197 (2006).

11. X. A. Cao, H. Piao, S. F. LeBoeuf, J. Li, J. Y. Lin, and H. X. Jiang, *Appl. Phys. Lett.*, **89**, 082109 (2006).
12. J. Neugebauer and C. G. Valle, *Appl. Phys. Lett.*, **69**, 503 (1996).
13. K. Saarinen, T. Laine, and S. Kuisma, *Phys. Rev. Lett.*, **79**, 3030 (1997).
14. G. S. Marlow and M. B. Das, *Solid-State Electron.*, **25**, 91 (1982).
15. K. A. Ricket, A. B. Ellis, F. J. Himpsel, J. Sun, and T. F. Kuech, *Appl. Phys. Lett.*, **80**, 204 (2002).
16. J.-S. Jang and T.-Y. Seong, *J. Appl. Phys.*, **88**, 3064 (2000).
17. T. Mattila and R. M. Nieminen, *Phys. Rev. B*, **55**, 9571 (1997).
18. B. Van Daele, G. Van Tendeloo, W. Ruythooren, J. Derluyn, M. R. Leys, and M. Germain, *Appl. Phys. Lett.*, **87**, 061905 (2005).
19. S. J. Pearton, J. C. Zolper, R. J. Shul, and F. Ren, *J. Appl. Phys.*, **86**, 1 (1999).
20. J.-S. Jang, C.-W. Lee, S.-J. Park, T.-Y. Seong, and I. T. Ferguson, *J. Electron. Mater.*, **31**, 903 (2002).
21. X. A. Cao, E. B. Stokes, P. M. Sandik, S. F. LeBoeuf, J. Kretchmer, and D. Walker, *IEEE Electron Device Lett.*, **23**, 535 (2002).
22. Y. B. Hahn, R. J. Choi, J. H. Hong, H. J. Park, C. S. Choi, and H. J. Lee, *J. Appl. Phys.*, **92**, 1189 (2002).
23. H. S. Yang, S. Y. Han, K. H. Baik, S. J. Pearton, and F. Ren, *Appl. Phys. Lett.*, **86**, 102104 (2005).
24. X. Guo and E. F. Schubert, *J. Appl. Phys.*, **90**, 4191 (2001).
25. H. Kim, S. J. Park, and H. Hwang, *Appl. Phys. Lett.*, **81**, 1326 (2002).
26. A. Chakraborty, L. Shen, and H. Masui, *Appl. Phys. Lett.*, **88**, 181120 (2006).